Voltage–Amplitude Response of Superharmonic Resonance of Second Order of Electrostatically Actuated MEMS Cantilever Resonators

Dumitru I. Caruntu[1]
Mechanical Engineering Department,
University of Texas Rio Grande Valley,
Edinburg, TX 78539
e-mails: dumitru.caruntu@utrgv.edu;
caruntud2@asme.org; dcaruntu@yahoo.com

Martin A. Botello
Mechanical Engineering Department,
University of Texas Rio Grande Valley,
Edinburg, TX 78539

Christian A. Reyes
Mechanical Engineering Department,
University of Texas Rio Grande Valley,
Edinburg, TX 78539

Julio S. Beatriz
Mechanical Engineering Department,
University of Texas Rio Grande Valley,
Edinburg, TX 78539

This paper investigates the voltage–amplitude response of superharmonic resonance of second order (order two) of alternating current (AC) electrostatically actuated micro-electromechanical system (MEMS) cantilever resonators. The resonators consist of a cantilever parallel to a ground plate and under voltage that produces hard excitations. AC frequency is near one-fourth of the natural frequency of the cantilever. The electrostatic force includes fringe effect. Two kinds of models, namely reduced-order models (ROMs), and boundary value problem (BVP) model, are developed. Methods used to solve these models are (1) method of multiple scales (MMS) for ROM using one mode of vibration, (2) continuation and bifurcation analysis for ROMs with several modes of vibration, (3) numerical integration for ROM with several modes of vibration, and (4) numerical integration for BVP model. The voltage–amplitude response shows a softening effect and three saddle-node bifurcation points. The first two bifurcation points occur at low voltage and amplitudes of 0.2 and 0.56 of the gap. The third bifurcation point occurs at higher voltage, called pull-in voltage, and amplitude of 0.44 of the gap. Pull-in occurs, (1) for voltage larger than the pull-in voltage regardless of the initial amplitude and (2) for voltage values lower than the pull-in voltage and large initial amplitudes. Pull-in does not occur at relatively small voltages and small initial amplitudes. First two bifurcation points vanish as damping increases. All bifurcation points are shifted to lower voltages as fringe increases. Pull-in voltage is not affected by the damping or detuning frequency. [DOI: 10.1115/1.4042017]

Keywords: superharmonic resonance of the second order, MEMS cantilever resonator, electrostatic actuation, voltage–amplitude response, method of multiple scales (MMS), reduced-order model (ROM), boundary value problem (BVP), fringe effect

1 Introduction

Micro-electromechanical systems (MEMS) such as microbeams utilize electrostatic force actuation in order to produce deflections [1]. The simplicity of MEMS design allows for a vast range of application such as resonators [2,3], switches [4,5], and sensors [6,7]. MEMS may operate in different conditions to best suit their application. For an example, the electrostatic force can be produced by either DC voltage, AC voltage, or both. DC voltage applications, such as micro-actuators, desire a static beam deflection in order to operate. On the contrary, microresonator applications require AC voltage, or AC and DC voltages, in order to obtain a vibrating beam [3,6]. The behavior of the MEMS structure can also be changed by using different boundary conditions of the beam, such as fixed-free and fixed-fixed, as well as using uniform cross section or nonuniform cross section. These different configurations regarding the applied voltage and the type of MEMS structure determine the dynamics of the system.

Investigations of the behavior, operating ranges, and limitations of MEMS resonators are necessary. Numerical simulations of different models can be used to investigate the dynamical behavior of the system. For an example, the mechanical response of MEMS cantilever resonator under an electrical load can be investigated using an Euler–Bernoulli beam model and Palmer formula model of the electrostatic force. Palmer formula is valid in the case of parallel plate capacitors. The fringe effect is an additional attracting force due to the electrical field outside the volume between the parallel plates of the MEMS [8]. This additional attraction force is not accounted for in the theory of electrostatic force for parallel plates capacitors. The fringe effect increases when the gap distance between the parallel plates increases and/or the width of the beam decreases. At the microlevel, fringe effect and viscous damping become significant and can have an important influence on the nonlinear behavior of the system [8,9]. Viscous damping describes the air resistance on the beam.

Fringe and viscous damping affect stability, i.e., bifurcation point and pull-in phenomena. This has a direct effect on device's sensitivity and operating range [10]. Models have been developed to predict the occurrence of these phenomena [11–14]. For instance, microcantilever beams driven by electrostatic and piezoelectric forces using the modified couple stress theory have been modeled and Galerkin method has been used for predicting static pull-in voltage [12].

Superharmonic resonance of second order (order two) of electrostatically actuated MEMS structures modeled as continuous systems has been reported in the literature by research groups of Nayfeh and coworkers [15–17], and Amabili and coworkers [3], and only for clamped–clamped microbeams (MEMS bridges). The voltage–amplitude response (force response) has been investigated by Abdel-Rahman and Nayfeh [16], Nayfeh and Younis [17], and Ghayesh et al. [3], only in the case of electrostatically

[1]Corresponding author.

Contributed by the Design Engineering Division of ASME for publication in the Journal of Computational and Nonlinear Dynamics. Manuscript received March 23, 2018; final manuscript received November 10, 2018; published online January 18, 2019. Assoc. Editor: Eihab Abdel-Rahman.

actuated MEMS bridge resonators with the actuating voltage including both components DC and AC, in which the DC voltage is much larger than the AC voltage. This led to superharmonic resonance for AC frequency near half natural frequency of the resonator. Najar et al. [15] investigated same electrostatically actuated MEMS bridge resonators under same conditions; they reported only the frequency-amplitude response. Lumped models of such structures have been reported by Al-Ghamdi et al. [18] and Alsaleem et al. [19].

All investigations in Refs. [3], [16], and [17] reported the same type of behavior (bifurcation diagram) of electrostatically actuated MEMS bridge resonators. The amplitude of the midpoint of the resonator increased along a stable branch with the increase of the AC voltage until it reached a saddle-node bifurcation point. The unstable branch connected this bifurcation point with another saddle-node bifurcation point located at higher amplitude and lower AC voltage. The stable branch of the second bifurcation point shows an increase in amplitude with the increase of AC voltage.

While Abdel-Rahman and Nayfeh [16] used the method of multiple scales (MMS), Nayfeh and Younis [17] and Ghayesh et al. [3], used reduced-order models (ROMs) to include 4 and 16 modes of vibration, respectively. However neither Ghayesh et al. [3] nor Nayfeh and Younis [17] reported a convergence criterion for determining the number of modes of vibration necessary in the model.

This work investigates the voltage–amplitude response of superharmonic resonance of second order of AC electrostatically actuated MEMS cantilever resonators. The DC voltage is negligible. The AC frequency is near one-fourth of the resonator's natural frequency. This work is a different case than Refs. [3] and [15–17] in terms of AC frequency, which is near one fourth of the natural frequency and not one half, boundary conditions, and negligible DC voltage. For this resonance to occur hard excitations are required, i.e., the amplitude of the AC voltage has to be significant. The superharmonic resonance is investigated using two types of models, ROMs to include one to several modes of vibration, and boundary value problem (BVP) model. The BVP model has not been reported in Refs. [3] and [15–17]. The methods used in this work for predicting the behavior of MEMS cantilever resonators are the MMS [20–22], numerical integration, and continuation and bifurcation analysis of ROMs [13,23,24].

The novelty of this work is that (1) it reports the nonlinear voltage–amplitude response of superharmonic resonance of second order of AC electrostatically actuated MEMS cantilever resonator; resonance due to AC frequency near one-fourth of the resonator's natural frequency and AC amplitudes in the range of hard excitations. (2) Two kinds of models, namely ROMs and BVP model, and three methods are used in this investigation, namely MMS for voltage–amplitude response, continuation and bifurcation analysis of ROMs for voltage–amplitude response using AUTO 07P, and numerical integration of ROMs and BVP model for time responses using MATLAB. (3) This work reports that MMS is valid for amplitudes less than 0.4 of the gap and unreliable beyond this point. ROM and BVP are valid for all range of amplitudes provided a sufficient number of terms (modes of vibration) for ROM, and small enough time-step for BVP model, are considered. In this work, five terms ROM and *timestep* of 0.0005 for BVP can accurately predict the voltage–amplitude response of the system. (4) Three saddle-node bifurcations are reported in the voltage–amplitude bifurcation diagram. So, as the voltage is swept up there is a significant jump in amplitude at a voltage lower than the pull-in voltage. (5) The influence of the damping, detuning frequency, and fringe effect on voltage–amplitude response are reported.

2 Differential Equation of Motion

The following dimensionless partial differential equation (PDE), and boundary and initial conditions describe the motion of electrostatically actuated Euler–Bernoulli cantilever resonators [2,22]

$$\begin{cases} \dfrac{\partial^2 u(z,\tau)}{\partial \tau^2}+\dfrac{\partial^4 u(z,\tau)}{\partial z^4}=-b^*\dfrac{\partial u(z,\tau)}{\partial \tau}+\dfrac{\delta V^2}{\left[1-u(z,\tau)\right]^2}+\dfrac{f\delta V^2}{\left[1-u(z,\tau)\right]} \\ u(0,\tau)=\dfrac{\partial u}{\partial z}(0,\tau)=\dfrac{\partial^2 u}{\partial z^2}(1,\tau)=\dfrac{\partial^3 u}{\partial z^3}(1,\tau)=0 \\ u(z,0)=f(z),\dfrac{\partial u}{\partial \tau}(z,0)=g(z) \end{cases} \tag{1}$$

where $u=u(z,\tau)$, z, and τ are dimensionless variables, namely transverse displacement (deflection) of the resonator, longitudinal coordinate, and time, respectively. The dimensionless variables are given by

$$u=\frac{w}{g};\quad z=\frac{x}{\ell};\quad \tau=t\cdot\frac{1}{\ell^2}\sqrt{\frac{EI_0}{\rho A_0}} \tag{2}$$

where w, x, and t are the corresponding dimensional variables, respectively, ℓ beam length, g gap between the cantilever and ground plate, ρ density, and E Young modulus. One should mention that in the numerical simulations of this work the steady-state amplitudes of the free end of the cantilever $U_{\max}$ are reported. For uniform structures, A_0 and I_0 are the cross section area and moment of inertia of the cantilever. Functions $f(z)$ and $g(z)$ are the initial deflection and velocity of the resonator. The dimensionless AC voltage considered in this work is $\delta\cdot V(\tau)$, where

$$V(\tau)=\cos\Omega^*\tau \tag{3}$$

The dimensionless parameters in Eq. (1) are b^*, δ, and f, namely damping parameter, voltage parameter, and fringe effect parameter; Ω^* is dimensionless frequency of excitation. They are given by

$$b^*=\frac{b\ell^2}{g\sqrt{\rho E A_0 I_0}},\ \delta=\frac{\varepsilon_0 W\ell^4 V_0^2}{2g^3 EI_0},\ f=\frac{0.65g}{W},\ \Omega^*=\Omega\ell^2\sqrt{\frac{\rho A_0}{EI_0}} \tag{4}$$

where b is a dimensional viscous damping per unit length coefficient, W is the beam width, ε_0 is the permittivity of free space, V_0 is the dimensional voltage amplitude, and Ω is the dimensional frequency of excitation. Figure 1 shows a uniform cantilever beam under electrostatic actuation.

Regarding damping, the quality factor Q and damping coefficient per unit length b (Table 1) are for conditions of squeeze film damping in rarefied gas [25]. One should mention that the fringe effect is described by Palmer formula [8,26]. Resonators in this work do not fall in the category of narrow beams.

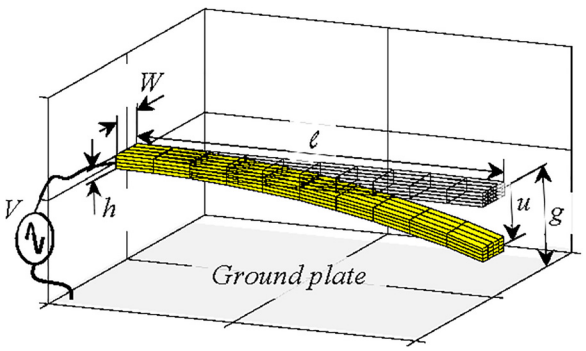

Fig. 1 Uniform cantilever MEMS resonator of constant thickness *t* and constant width *W*, and under electrostatic actuation due to AC voltage $V_0\cos\Omega t$

3 Superharmonic Resonance of Second-Order

The dimensionless frequency of the AC voltage between MEMS cantilever resonator and the parallel ground plate is near one fourth of the first natural frequency ω_1 of the resonator, $\Omega^* \approx \omega_1/4$. This can be written as

$$\Omega^* = \frac{\omega_1}{4} + \varepsilon\sigma \tag{5}$$

where σ is the detuning frequency parameter, and ε is a dimensionless parameter used as bookkeeping device in MMS to indicate small terms of the equation. For this resonance to occur, the voltage parameter δ should be large enough to produce hard excitations, as shown afterward.

4 Method of Multiple Scales

The method of multiple scales is used in this work to investigate the superharmonic resonance of second order of electrostatically actuated cantilever resonators. The solution of Eq. (1), where the nonlinear electrostatic force and fringe effect are expanded in Taylor series to the cubic power, is assumed to be

$$u = u_1(\tau)\phi_1(z) \tag{6}$$

where ϕ_1 is the first mode shape, and u_1 is a function of time to be determined. Mode shapes ϕ_i [19,24], satisfy the following equations:

$$\phi_i^{(4)}(z) = \omega_i^2\phi_i(z)\,, \quad \int_0^1 \phi_i(z)\phi_j(z)dz = \delta_{ij} = \begin{cases} 0, & i \neq j \\ 1, & i = j \end{cases} \tag{7}$$

where ω_i are the corresponding natural frequencies, and δ_{ij} is Kronecker's delta [14]. Using Eqs. (6) and (7), along with the inclusion of the Taylor expansion of the electrostatic force and fringe effect up to the cubic power, in Eq. (1), it results in

$$\begin{aligned} &\ddot{u}_1\phi_1 + \omega_1^2 u_1\phi_1 + \varepsilon b^*\dot{u}_1\phi_1 = \delta V^2(1+f) \\ &\quad +\varepsilon\delta V^2[(2+f)u_1\phi_1 + (3+f)u_1^2\phi_1^2 + (4+f)u_1^3\phi_1^3] \end{aligned} \tag{8}$$

To model the hard excitation of the system, the first term on the right-hand side of Eq. (8) does not contain the bookkeeping parameter ε [20–22]. The bookkeeping parameter indicates small terms in Eq. (8). If one wants to model soft excitations, which is not the purpose of this work, then the first term of the right-hand side of Eq. (8) should contain ε as well. An MMS uniform expansion of the transverse displacement u_1 [2], is assumed as

$$u_1 = u_{10}(T_0, T_1) + \varepsilon u_{11}(T_0, T_1) \tag{9}$$

where $T_0 = t$ and $T_1 = \varepsilon t$ are fast-time scale and slow-time scale, respectively [24,27]. Using Eqs. (3) and (5), the square of the dimensionless voltage is given by

$$V^2 = \frac{1}{2} + \frac{1}{4}\left(e^{\frac{i\omega_1 T_0}{2}}e^{2i\sigma T_1} + e^{\frac{-i\omega_1 T_0}{2}}e^{-2i\sigma T_1}\right) \tag{10}$$

The time derivatives, in terms of T_0 and T_1, are given by

$$\begin{aligned} &\frac{\partial}{\partial t} = D_0 + \varepsilon D_1, \quad \frac{\partial^2}{\partial t^2} = D_0^2 + 2\varepsilon D_0 D_1 + \varepsilon^2 D_1^2, \text{ where} \\ &D_n = \frac{\partial}{\partial T_n}, n = 1, 2 \end{aligned} \tag{11}$$

Substituting Eqs. (9) and (11) into Eq. (8), multiplying the resulting equation by $\phi_1(z)$ and integrating from 0 to 1, and then equating the coefficients of the same powers of ε, the following two problems, namely zero-order and first-order, result:

Table 1 Dimensional system parameters

Beam width	W	20 μm
Beam length	ℓ	300 μm
Beam thickness	h	2.0 μm
Initial gap distance	g	8.0 μm
Material density	ρ	2330 kg/m^3
Young's modulus	E	169 GPa
Permittivity of free space	ε_0	8.854×10^{-12} C^2/N m^2
Quality factor	Q	4200
Peak AC voltage	V_0	28.36 V

$$\varepsilon^0:\ D_0^2 u_{10} + \omega_1^2 u_{10} = \delta V^2(1+f)g_0 \tag{12}$$

$$\begin{aligned} \varepsilon^1:\ &D_1^2 u_{11} + \omega_1^2 u_{11} = -2D_0 D_1 u_{10} - b^* D_0 u_{10} \\ &+\delta V^2[(2+f)u_{10} + (3+f)u_{10}^2 g_2 + (4+f)u_{10}^3 g_3] \end{aligned} \tag{13}$$

where

$$g_n = \int_0^1 \phi_1^{n+1} dz \qquad n = 1, 2, 3, 4 \tag{14}$$

and $g_1 = 1$. The general solution of the nonhomogenous Eq. (12) is given by

$$\begin{aligned} u_{10} = &\left[A(T_1)e^{i\omega_1 T_0} + \bar{A}(T_1)e^{-i\omega_1 T_0}\right] \\ &+ \left[\Lambda e^{\frac{i\omega_1 T_0}{2} + 2i\sigma T_1} + \Lambda e^{\frac{-i\omega_1 T_0}{2} - 2i\sigma T_1}\right] + K \end{aligned} \tag{15}$$

where A and $\bar{A}$ are complex conjugate coefficients to be determined. These coefficients depend on the slow time scale T_1. Coefficients Λ and K are as follows:

$$\Lambda = \frac{\delta g_0(1+f)}{4\left(\omega_1^2 - 4\Omega^2\right)}, \qquad K = \frac{\delta g_0(1+f)}{2\omega_1^2} \tag{16}$$

Substituting Eqs. (15) and (10) into Eq. (13), collecting the secular terms $(e^{i\omega_1 T_0})$, and setting their sum to equal to zero, the following equation results:

$$\begin{aligned} &-2i\omega_1 A' - i\omega_1 b^* A + \delta\left[\frac{1}{2}(2+f)A + \frac{1}{2}(3+f)(\Lambda^2 e^{4i\sigma T_1} + 2AK)g_2\right. \\ &+\frac{1}{2}(4+f)(3A^2\bar{A} + 6A\Lambda^2 + 3AK^2 + 3K\Lambda^2 e^{4i\sigma T_1})g_3 \\ &+\frac{1}{4}(2+f)\Lambda e^{4i\sigma T_1} + \frac{1}{4}(3+f)(4A\Lambda + 2\Lambda e^{4i\sigma T_1})g_2 \\ &+\frac{1}{4}(4+f)(6A\bar{A}\Lambda e^{4i\sigma T_1} + 4\Lambda^3 e^{4i\sigma T_1} + 12A\Lambda K \\ &\left.+3K^2\Lambda e^{4i\sigma T_1} + 3A^2\Lambda e^{-4i\sigma T_1})g_3\right] = 0 \end{aligned} \tag{17}$$

where A' is the derivative of A with respect to the slow time scale T_1. Then, A is expressed in polar form as

$$A = \frac{1}{2}ae^{i\beta} \tag{18}$$

where a is the real amplitude, and β is the real phase. Substituting Eq. (18) into Eq. (17) and separating the real (Re) and imaginary (Im) parts, the steady-state amplitudes, corresponding to $(a' = 0, \gamma' = 0)$, of the (δ, a) voltage–amplitude response (bifurcation diagram) are given by

$$\sigma = -\frac{\delta}{4\omega_1}\left[\frac{1}{4}(2+f)+\frac{1}{2}(3+f)(K+\Lambda)g_2+(4+f)\times\left(\frac{3}{16}a^2+\frac{3}{4}K^2+\frac{3}{2}\Lambda^2+\frac{3}{2}\Lambda K\right)g_3\right] - \frac{\delta\Lambda\cos\gamma}{4\omega_1 a}\left[\frac{1}{4}(2+f)+\frac{1}{2}(3+f)(\Lambda+K)g_2+(4+f)\times\left(\frac{9}{16}a^2+\frac{3}{4}K^2+\Lambda^2+\frac{3}{2}\Lambda K\right)g_3\right] \tag{19}$$

and

$$0 = -\frac{1}{2}b^* a\omega_1+\delta\Lambda\sin\gamma\left[\frac{1}{4}(2+f)+\frac{1}{2}(3+f)(\Lambda+K)g_2+(4+f)\left(\frac{3}{16}a^2+\frac{3}{4}K^2+\Lambda^2+\frac{3}{2}\Lambda K\right)g_3\right] \tag{20}$$

where

$$\gamma = 4\sigma T_1-\beta,\ \gamma' = 4\sigma-\beta' \tag{21}$$

Equations (19) and (20) are parametric equations, where the parameter is γ. For a given detuning frequency σ, the amplitude a, and voltage δ are numerically determined from Eqs. (19) and (20). One should mention that the amplitude of the tip of the resonator is $U_{\max} = a\phi_1(1)$.

5 Reduced-Order Model

A set of nonexplicit ordinary differential equations are developed by using ROM [13,14,23,24] to include several modes of vibration. "Methods in the class of domain methods such as ROM eliminate the spatial dependence in the PDEs using the Galerkin method. The displacement is expressed as a linear combination of a complete set of linearly independent basis functions ϕ_i in the form

$$u(z,\tau) = \sum_{i=1}^{N} u_i(\tau)\phi_i(z) \tag{22}$$

where $u_i(\tau)$ are the generalized coordinate associated with basis functions ϕ_i," [13]; $u_i(\tau)$ are time-dependent functions to be determined. In this work $N = 2,3,4,5$ and it is the number of ROM terms (modes of vibration), and ϕ_i are the linear undamped mode shapes of uniform cantilever beams [13,24]. The mode shapes satisfy Eq. (8). ROM is implemented after multiplying the dimensionless equation of motion Eq. (1) by $(1-u)^2$ in order to eliminate any displacement terms from appearing in the denominators [2,13,14,17]. Substituting Eq. (22) into the resulting PDE, and "requiring the residue to be orthogonal to every basis function, we obtain n second-order ordinary differential equations (ODEs) in time in terms of the generalized coordinates $u_i(\tau)$" [13]. Therefore, Eq. (22) is substituted into the resulting equation, which is then multiplied by $\phi_n(z)$ and integrated from $z = 0$ to 1, where $n = 1,2,\ldots,N$. This results in a system of N second-order ODEs given by

$$\sum_{i=1}^{N}\ddot{u}_i h_{ni}-2\sum_{i,j=1}^{N}\ddot{u}_i u_j h_{nij}+\sum_{i,j,k=1}^{N}\ddot{u}_i u_j u_k h_{nijk}+\sum_{i=1}^{N}\omega_i^2 u_i h_{ni} -2\sum_{i,j=1}^{N}\omega_i^2 u_i u_j h_{nij}+\sum_{i,j,k=1}^{N}\omega_i^2 u_i u_j u_k h_{nijk} +b^*\sum_{i=1}^{N}\dot{u}_i h_{ni}-2b^*\sum_{i,j=1}^{N}\dot{u}_i u_j h_{nij}+b^*\sum_{i,j,k=1}^{N}\dot{u}_i u_j u_k h_{nijk} = \delta V^2[(1+f)h_n+f\sum_{i=1}^{N}u_i h_{ni}] \tag{23}$$

where $n = 1,2,\ldots,N$, and $i,j,k = 1,2,\ldots,N$. The coefficients h are as follows:

$$h_n = \int_0^1 \phi_n dz\,,\ h_{ni} = \int_0^1 \phi_n\phi_i dz\,,\ h_{nij} = \int_0^1 \phi_n\phi_i\phi_j dz\,,\ h_{nijk} = \int_0^1 \phi_n\phi_i\phi_j\phi_k dz \tag{24}$$

The system of N second-order ODEs, Eq. (23), where $n = 1,2,\ldots,N$, is then transformed into a system of first-order ODEs as follows:

$$\begin{cases}\dot{y}(2k-1) = y(2k)\\ \dot{y}(2k) = \ddot{u}_k\end{cases},\ k = 1,2,\ldots,N \tag{25}$$

by using the variables

$$\begin{cases}y(2k-1) = u_k\\ y(2k) = \dot{u}_k\end{cases},\ k = 1,2,\ldots,N \tag{26}$$

AUTO 07P, a software package for continuation and bifurcation problems [28], is then used for obtaining the voltage–amplitude response for cases of $N = 2,3,4,5$, Eq. (25). In this work, time responses of 5T ROM for specified parameters are also obtained using a MATLAB ODE solver, namely *ode15s*. One should mention that *ode15s* is a "multistep, variable order solver based on numerical differentiation formulas" [29,30].

6 Boundary Value Problem

Boundary value problem model is also used to investigate the nonlinear voltage–amplitude response of the MEMS cantilever resonator. Equation (1) can be written as

$$\frac{\partial^4 u}{\partial z^4} = -\frac{\partial^2 u}{\partial\tau^2}-b^*\frac{\partial u}{\partial\tau}+\frac{\delta}{(1-u)^2}V^2(\tau)+\frac{f\delta}{(1-u)}V^2(\tau) \tag{27}$$

where V is given by Eq. (3), and the boundary conditions are given by Eq. (1). The initial conditions used in this work are as follows:

$$u(z,0) = U_0\frac{\phi_1(z)}{\phi_1(0)},\quad \frac{\partial u}{\partial\tau}(z,0) = 0 \tag{28}$$

where U_0 is the initial deflection of the tip of the MEMS resonator, and $\phi_1(0) = 2$. Consider a time sequence $(\tau)_n$ and denote $u(z,\tau_n) = u_n(z)$. Difference quotients are used for the time partial derivates and are as follows:

$$\frac{\partial^2 u}{\partial\tau^2}(z,\tau_n) = \frac{u_n-2u_{n-1}+u_{n-2}}{(\Delta\tau)^2},\ \frac{\partial u}{\partial\tau}(z,\tau_n) = \frac{u_n-u_{n-2}}{2\Delta\tau} \tag{29}$$

where $u_n(z)$ has been denoted by u_n. A fourth-order ordinary differential equation with respect to z results for each step in time τ_n, by substituting Eq. (29) into Eq. (27). The fourth-order ODE is then transformed into a system of four first-order ODEs by introducing four new variables as follows:

$$y_{1,n} = u_n, y_{2,n} = \frac{du_n}{dz}, y_{3,n} = \frac{d^2u_n}{dz^2}, y_{4,n} = \frac{d^3u_n}{dz^3} \tag{30}$$

The resulting system of first-order differential equations is given by

$$\begin{cases} y'_{1,n} = y_{2,n}\\ y'_{2,n} = y_{3,n}\\ y'_{3,n} = y_{4,n}\\ y'_{4,n} = -\dfrac{y_{1,n}-2y_{1,n-1}+y_{1,n-2}}{(\Delta\tau)^2}-b^*\dfrac{y_{1,n}-y_{1,n-2}}{2\Delta\tau}\\ \quad+\dfrac{\delta}{(1-y_{1,n})^2}\cos^2(\Omega\cdot\tau_n)+\dfrac{f\delta}{(1-y_{1,n})}\cos^2(\Omega\cdot\tau_n)\end{cases} \tag{31}$$

where $'$ denotes derivative with respect to z and $n = 3, 4, 5, \ldots$. The boundary conditions are

$$y_{1,n}(0) = y_{2,n}(0) = y_{3,n}(1) = y_{4,n}(1) = 0 \tag{32}$$

where $n = 1, 2, 3, \ldots$. The initial conditions, given by Eq. (28), provide the deflections $y_{1,1}$ and $y_{1,2}$ for τ_1 and τ_2. The boundary value problem given by Eqs. (31) and (32) is solved using *bvp4c*, a boundary value problem solver of MATLAB, for each step in time τ_n, $n = 3, 4, 5, \ldots$. "This solver is based on the three-stage Labatto formula which is a collocation formula. The collocation polynomial provides a solution that is a fourth-order accurate uniformly," [31], in the interval $[0, 1]$ in our case.

7 Numerical Results

Numerical simulations are conducted for a typical MEMS cantilever resonator with geometry and material shown in Tables 1 and dimensionless parameters shown in Table 2. The mode shapes ϕ_i for a uniform cantilever [24] are as follows:

$$\phi_i(z) = -\{\cos(\sqrt{\omega_i}z) - \cosh(\sqrt{\omega_i}z) + C_i[\sin(\sqrt{\omega_i}z) - \sinh(\sqrt{\omega_i}z)]\} \tag{33}$$

where the first five natural frequencies ω_i and constant coefficients C_i are given in Table 3. The calculated g coefficients for Eq. (14) are given in Table 4. All numerical simulations are conducted in the case of AC frequency near one fourth of the first natural frequency, Eq. (5) for n=1.

Microelectromechanical system cantilever resonator under superharmonic resonance of second-order is investigated using two models, namely ROMs and BVP model in order to predict the nonlinear voltage–amplitude response. Three methods of solving these models are used, namely MMS, numerical integration, and continuation and bifurcation analysis. An investigation was conducted on the convergence of ROMs with the number of modes of vibration, up to five modes. The effects on the voltage–amplitude response of various parameters, such as damping b^*, fringe f, and detuning frequency σ, are reported.

Figure 2 shows the voltage–amplitude response of MEMS resonator in accordance to MMS, five-term ROM (using AUTO 07P software for voltage–amplitude response 5T AUTO, and MATLAB solver *ode15s* for time responses 5T TR), and BVP model using MATLAB solver *bvp4c* for time responses BVP4C. Solid and dashed branches represent the stable and unstable steady-state solutions, respectively. The system experiences a softening effect, in which the branches are bent to the left at relative high amplitudes. For voltages greater than the voltage of point C and any initial amplitude, and for initial amplitudes above the unstable branch of CD and any voltage between the voltages of points C and D, the system experiences pull-in instability, i.e., the tip of the resonator makes contact with the parallel ground plate. The three methods are in agreement at voltages lower than $\delta = 0.3$. However, for voltage greater than $\delta = 0.3$, MMS is not in agreement with ROMs (5T AUTO and 5T time responses) and BVP time responses. MMS predicts erroneous voltage–amplitude responses. This disagreement is due to the fact that MMS solves one mode of vibration (term) ROM and uses only up to cubic terms of the Taylor expansion of the electrostatic force [2,22], while numerical integration is used for five terms ROM, and refined enough time mesh for the BVP model. It has been reported in the literature that ROM using three or more modes guarantees the convergence of the steady-state amplitudes, and accurately captures the behavior of the system where MMS could not [23,24], i.e., in the case of amplitudes larger than half the gap and less than the pull-in instability limit. BVP and ROM are slightly different between $0.4 < \delta < 0.8$, where the softening effect is present. However, for $0.8 \leq \delta \leq 1.615$, BVP and 5T ROM are in agreement for the voltage–amplitude response. For initial amplitudes greater than unstable branch CD, BVP and 5T ROM are in agreement. The steady-state amplitudes of 5T AUTO, the ROM continuation and bifurcation analysis using AUTO 07P, and the time responses resulting from numerical integration, MATLAB solver *ode15s*, are in agreement throughout the entire range of the voltage–amplitude responses.

One can notice that for the given $\sigma = -0.025$, pull-in is experienced when (1) the voltage is between $0.282 < \delta < 1.615$ and the initial amplitude is above the unstable branch CD, or (2) for voltages greater than $\delta = 1.615$ regardless of the initial amplitude. For any other voltage values, the MEMS resonator will settle to amplitudes on the stable branches (solid lines) regardless of the initial amplitude. It is also shown that at $\delta = 0$, the steady-state amplitude is zero, i.e., the resonator will not move if no voltage is applied. When the voltage is swept up, the amplitude increases until it reaches the saddle-node bifurcation point A. At this point, the amplitude jumps up from 0.223 of the gap to about 0.5 on the stable branch BC. Then, the amplitude decreases to about 0.2 of the gap at $\delta = 0.8$. Next, the amplitude begins to increase again until it reaches the saddle-node bifurcation point C. At this point, the system loses stability and the amplitude jumps to 1 (pull-in). For any voltage greater than the pull-in voltage δ_C, the system experiences pull-in regardless of the initial amplitude.

Figures 3–7, each figure having four subplots, show time responses of the electrostatically actuate MEMS cantilever resonator for $\sigma = -0.025$, $b^* = 0.01$, and $f = 0.26$, for different initial amplitudes and different voltage parameter values, using ROM approach in Figs. 3–6, and BVP approach in Fig. 7. Figures 3–6 have initial amplitudes of $U_0 = 0$, $U_0 = 0.4$, $U_0 = 0.7$, and

Table 2 Dimensionless system parameters

Damping parameter	b^*	0.01
Detuning parameter	σ	−0.025
Fringe correction parameter	f	0.26

Table 3 First five natural frequencies and constant coefficients for uniform cantilever

	$i = 1$	$i = 2$	$i = 3$	$i = 4$	$i = 5$
ω_i	3.51605	22.03449	61.69721	120.90192	199.85953
C_i	−0.73410	−1.01847	−0.99922	−1.00003	−0.99999

Table 4 g Coefficients for Eq. (16)

	$n = 0$	$n = 1$	$n = 2$	$n = 3$
g_n	0.7830	1.0000	1.4778	2.3487

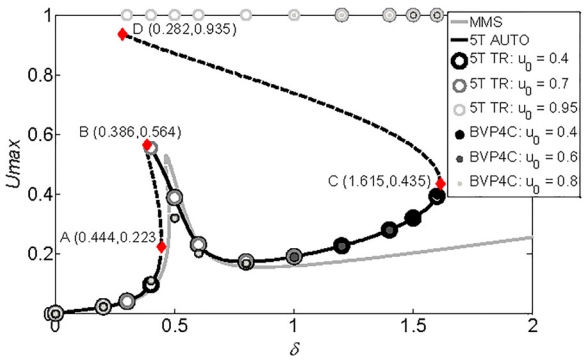

Fig. 2 Voltage–amplitude response using MMS, 5T AUTO, and 5T TR; $b^* = 0.01$, $f = 0.26$, $\sigma = -0.025$

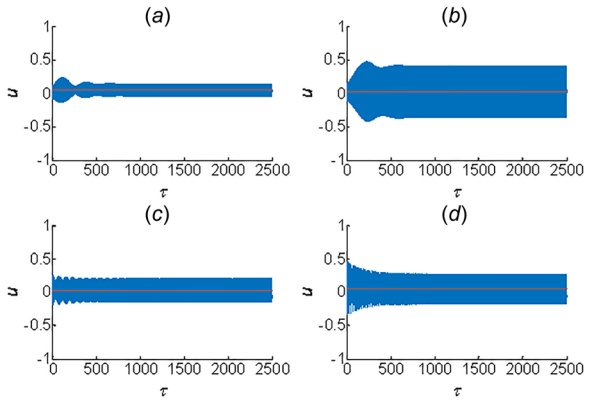

Fig. 3 Time responses using five term ROM (5T TR); $\sigma = -0.025$, $U_0 = 0$, $b^* = 0.01$, $f = 0.26$, (*a*) $\delta = 0.4$, (*b*) $\delta = 0.5$, (*c*) $\delta = 0.8$, and (*d*) $\delta = 1.2$

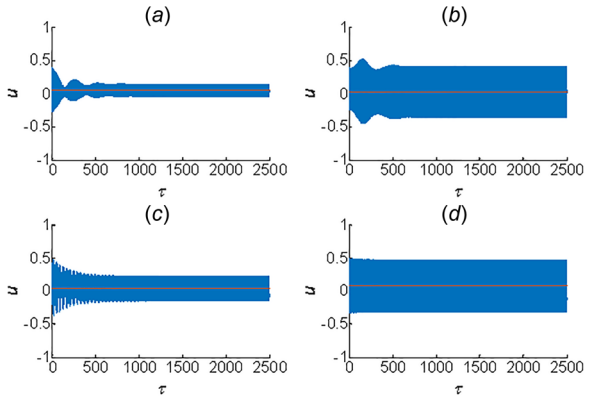

Fig. 4 Time responses using five term ROM (5T TR); $\sigma = -0.025$, $U_0 = 0.4$, $b^* = 0.01$, $f = 0.26$, (*a*) $\delta = 0.4$, (*b*) $\delta = 0.5$, (*c*) $\delta = 1.0$, and (*d*) $\delta = 1.6$

$U_0 = 0.95$, respectively, and each one various voltage parameter values, while Fig. 7 has one voltage parameter value, and four initial amplitudes.

Figures 3(*a*) and 3(*b*) show time responses for $\delta = 0.4$ and $\delta = 0.5$, respectively, and initial amplitude $U_0 = 0$. One can notice that the voltage parameter value $\delta_A = 0.444$ of the saddle-node bifurcation point A is between the two δ values in Figs. 3(*a*) and 3(*b*). These time responses are in agreement with the predictions of 5T ROM AUTO, Fig. 2, showing that the system settles to steady-state amplitudes on stable branches OA and BC, and therefore they do not contradict the existence of the saddle-node bifurcation point A.

Figures 3(*c*) and 3(*d*) illustrate time responses for $\delta = 0.8$ and $\delta = 1.2$, respectively, and initial amplitude $U_0 = 0$. They are in agreement with 5T ROM AUTO. The system settles to steady-state amplitudes on stable branch BC, Fig. 2.

Figures 4(*a*) and 4(*b*) show time responses for $\delta = 0.4$ and $\delta = 0.5$, respectively, and initial amplitude $U_0 = 0.4$. These time responses are in agreement with the predictions of 5T ROM AUTO. The system settles to steady-state amplitudes on branches stable branches OA and BC, Fig. 2. Therefore, they do not disprove the existence of the saddle-node bifurcation point A.

Figures 4(*c*) and 4(*d*) illustrate time responses for $\delta = 1.0$ and $\delta = 1.6$, respectively, and initial amplitude $U_0 = 0.4$. The steady-state amplitudes of these responses are in agreement with the existence of stable branch BC in Fig. 2. One can see that the system settles to amplitudes on this branch.

Figures 5(*a*) and 5(*b*) show time responses for $\delta = 0.3$ and $\delta = 0.4$, respectively, and initial amplitude $U_0 = 0.7$. One can notice that the voltage parameter value $\delta_B = 0.386$ of the saddle-node bifurcation point B is between the two δ values in Figs. 5(*a*) and 5(*b*). These time responses are in agreement with the predictions of 5T ROM AUTO, Fig. 2. The system settles to steady-state amplitudes on stable branches OA and BC, and therefore, they do not negate the existence of the saddle-node bifurcation points A and B.

Figures 5(*c*) and 5(*d*) illustrate time responses for $\delta = 1.0$ and $\delta = 1.2$, respectively, and initial amplitude $U_0 = 0.7$. These responses are in agreement with the existence of the unstable branch CD, Fig. 2. One can see that the system settles to steady-state amplitude on branch BC if the initial amplitude is below unstable branch CD, Fig. 5(*c*), and goes to pull in if the initial amplitude is above branch CD, Fig. 5(*d*). These responses do not contradict the existence of the saddle-node bifurcation point C.

Figures 6(*a*) and 6(*b*) show time responses for $\delta = 0.2$ and $\delta = 0.3$, respectively, and initial amplitude $U_0 = 0.95$. One can notice that the voltage parameter value $\delta_D = 0.282$ of the unstable point D is between the two δ values in Figs. 6(*a*) and 6(*b*). These time responses are in agreement with the predictions of 5T ROM AUTO, Fig. 2. The system settles to an amplitude on stable branch OA if the voltage is less than δ_D, although the system starts from a large initial amplitude. Conversely the system goes into pull-in if the voltage is greater than δ_D, and the initial amplitude is above the unstable branch CD. Therefore, these responses do not disprove the existence of the unstable point D.

Figures 6(*c*) and 6(*d*) illustrate time responses for $\delta = 0.8$ and $\delta = 1.6$, respectively, and initial amplitude $U_0 = 0.95$. These responses are in agreement with the existence of the unstable

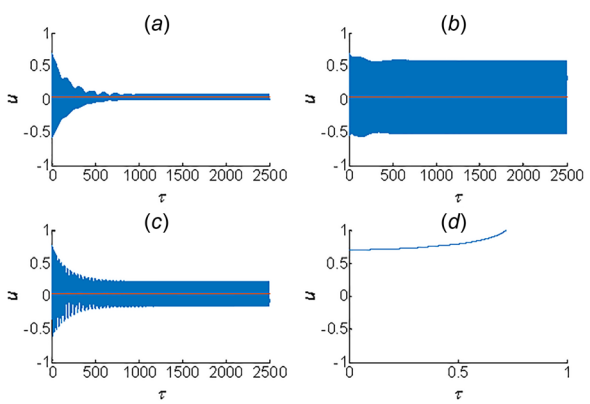

Fig. 5 Time responses using five term ROM (5T TR); $\sigma = -0.025$, $U_0 = 0.7$, $b^* = 0.01$, $f = 0.26$, (*a*) $\delta = 0.3$, (*b*) $\delta = 0.4$, (*c*) $\delta = 1.0$, and (*d*) $\delta = 1.2$

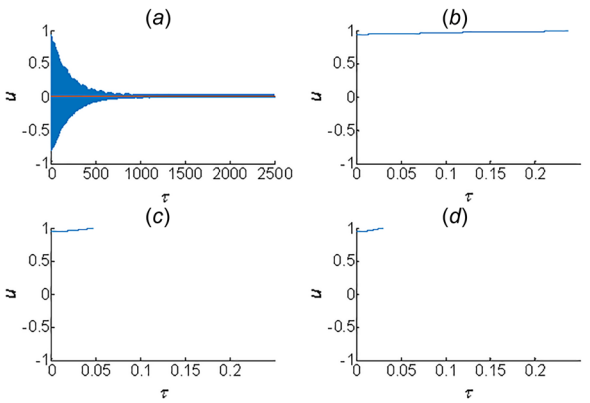

Fig. 6 Time responses using five term ROM (5T TR); $\sigma = -0.025$, $U_0 = 0.95$, $b^* = 0.01$, $f = 0.26$, (*a*) $\delta = 0.2$, (*b*) $\delta = 0.3$, (*c*) $\delta = 0.8$, and (*d*) $\delta = 1.6$

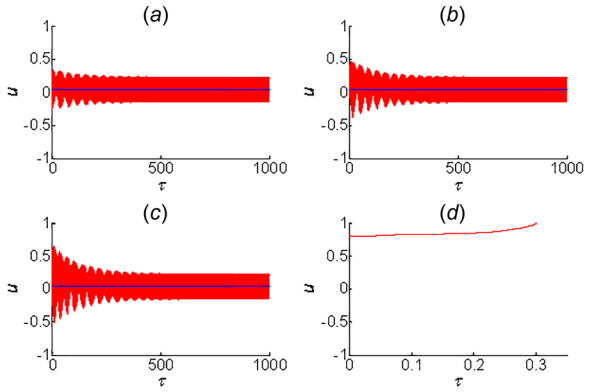

Fig. 7 Time responses using BVP4C with timestep = 0.0005; $\delta = 1.0$ $b^* = 0.01$, $f = 0.26$, $\sigma = -0.025$, (*a*) $U_0 = 0$, (*b*) $U_0 = 0.4$, (*c*) $U_0 = 0.6$, and (*d*) $U_0 = 0.8$

branch *CD*, Fig. 2. The system goes to pull in as the initial amplitude is above branch *CD*. These responses do not contradict the existence of the saddle-node bifurcation point *C*.

Figures 7(*a*)–7(*d*) show time responses using BVP approach for $\delta = 1.0$ and initial amplitudes of $U_0 = 0$, $U_0 = 0.4$, $U_0 = 0.6$, and $U_0 = 0.8$, respectively. One can notice that amplitude of the system settles on stable branch *BC* as long as the initial amplitude is below the unstable branch CD, and experiences pull-in if the initial amplitude is above the unstable branch *CD*. These time responses are in agreement with the predictions of 5T ROM AUTO, Fig. 2.

Figure 8 shows the convergence of voltage–amplitude response using MMS, two, three, four, and five term AUTO. MMS is included because it is equivalent to the one-term ROM. Five-term ROM gives the best predictions of the system's behavior.

Figure 9 shows the influence of the damping parameter b^* on the voltage–amplitude response of MEMS resonator. As damping increases, the peak amplitude and the amplitude of the saddle-node bifurcation point *B* decrease to the point where the softening effect vanishes and the system experiences a linear behavior. At low ($\delta < 0.4$) and high ($\delta > 0.7$) voltage values, damping does not affect the voltage–amplitude response.

Figure 10 shows the influence of the fringe parameter f on the voltage–amplitude response of MEMS resonator. As the fringe parameter increases, the response has a horizontal and vertical shift toward lower voltage and higher amplitude, respectively. Therefore, point *C* shifts toward lower voltage, therefore pull-in is experienced at lower voltages.

Figure 11 shows the influence of the detuning frequency parameter σ on the voltage–amplitude response of MEMS resonator. By

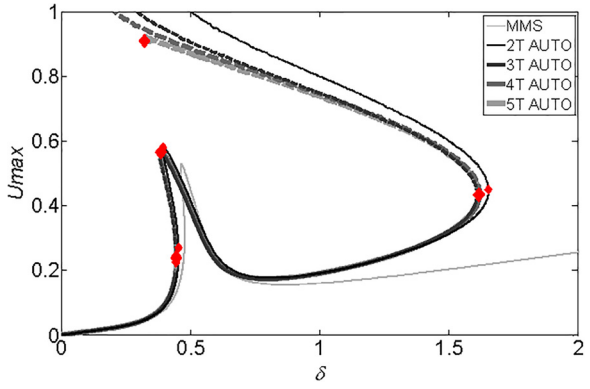

Fig. 8 Convergence of voltage–amplitude response using two, three, four, and five term ROM; MMS is included; $b^* = 0.01$, $f = 0.26$, $\sigma = -0.025$

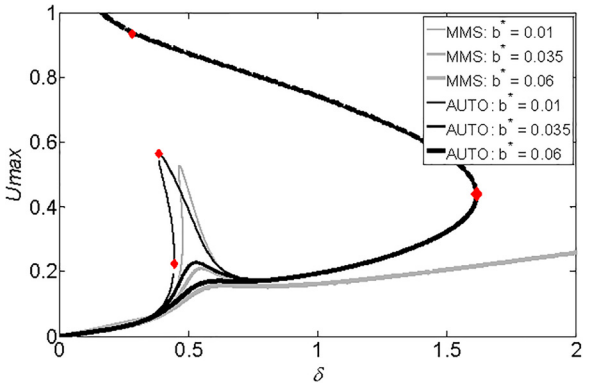

Fig. 9 Effect of damping parameter b* on the voltage–amplitude response using MMS and 5T AUTO; $f = 0.26$, $\sigma = -0.025$

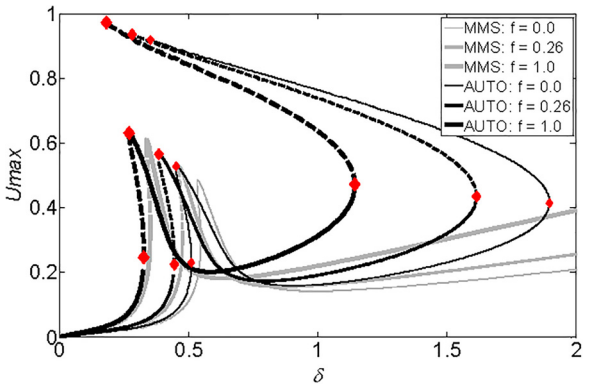

Fig. 10 Effect of fringe parameter f on the voltage–amplitude response using MMS and 5T AUTO; $b^* = 0.01$, $\sigma = -0.025$

increasing the detuning frequency parameter, point *A* is shifted toward lower voltage, while point *B* is vertically shifted toward smaller amplitudes. At low ($\delta < 0.2$) and high ($\delta > 1.2$) voltage values, the detuning frequency parameter does not influence the voltage–amplitude response.

8 Discussion and Conclusions

In this work, the voltage–amplitude response for AC electrostatically actuated MEMS cantilever resonators under superharmonic resonance of the second-order is investigated. MMS, numerical integration of ROMs and BVP model, and continuation and bifurcation analysis are used in this investigation. The AC frequency is near one-fourth of the resonator's natural frequency and

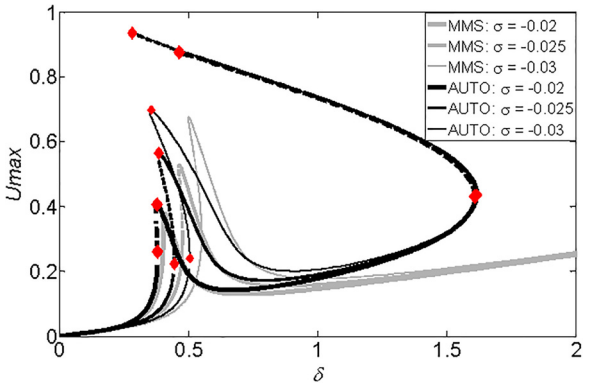

Fig. 11 Effect of detuning frequency σ on the voltage–amplitude response using MMS and 5T AUTO; $b^* = 0.01$, $f = 0.26$

the AC amplitude in the range of hard excitations. The system experiences characteristics of softening effect. Three saddle-node bifurcations are reported in the voltage–amplitude bifurcation diagram. So, as the voltage is swept up there is another significant jump in amplitude at a voltage lower than the pull-in voltage. If the dimensionless voltage δ is greater than 1.615, the system experiences pull-in regardless of initial amplitude. The effects of the damping b^*, fringe f, and detuning σ parameters on the voltage–amplitude response are also reported. As damping increases, the peak amplitude for low voltage decreases, and the bifurcation points A and B vanish, so the system approaches a linear behavior. As the fringe parameter increases, the steady-state amplitudes, i.e., bifurcation branches, translate toward lower voltage. Increasing detuning frequency parameter, the bifurcation branches shift toward lower voltage.

The numerical simulations in this work are valid for cantilever resonators that are not considered narrow structures, as the fringe effect was modeled by Palmer's formula. This formula is inaccurate when the width-to-thickness and gap-to-thickness ratios are between 0.5 and 5, and 0.2 and 2, respectively, Ref. [8]. The corresponding ratios in this work are 10 and 4, so the numerical results are valid. However, for narrow structures other models describing the fringe effect are reported [8].

The results of this paper are valid for long, slender cantilevers with a length-to-thickness ratio greater than 100 [32], as Euler–Bernoulli beam theory is used to model the MEMS resonator cantilever. In this work, this ratio is 150.

This work is only valid for uniform cantilevers. For nonuniform structures and their dynamic modal characteristics, or methods of finding these characteristics, are reported by Caruntu [33–35].

The simulations of this work are valid only for squeeze damping in rarefied gas [25,36–38]. The energy transfer model of the quality factor [25], along with the MEMS resonator characteristics in Table 1 to include the value of the quality factor, gives the value of damping parameter in Table 2. For the first mode of vibration, as in this paper, this corresponds to a pressure of about 130 Pa.

A limitation of this paper is that it does not include experimental work.

Future work could include the influence of Casimir effect in NEMS resonator system.

References

[1] Zhang, W.-M., Yan, H., Peng, Z. K., and Meng, G., 2014, "Electrostatic Pull-in Instability in MEMS/NEMS: A Review," Sens. Actuators A: Phys., **214**, pp. 187–218.

[2] Caruntu, D. I., Martinez, I., and Knecht, M. W., 2016, "Parametric Resonance Voltage Response of Electrostatically Actuated Micro-Electro-Mechanical System Cantilever Resonators," J. Sound Vib., **362**, pp. 203–213.

[3] Ghayesh, M. H., Farokhi, H., and Amabili, M., 2013, "Nonlinear Behaviour of Electrically Actuated MEMS Resonators," Int. J. Eng. Sci., **71**, pp. 137–155.

[4] LaRose, R. P., III., and Murphy, K. D., 2010, "Impact Dynamics of MEMS Switches," Nonlinear Dyn., **60**(3), pp. 327–339.

[5] Persano, A., Quaranta, F., Martucci, M. C., Siciliano, P., and Cola, A., 2015, "On the Electrostatic Actuation of Capacitive RF MEMS Switches on GaAs Substrate," Sens. Actuators A, **232**, pp. 202–207.

[6] Bogue, R., 2013, "Recent Developments in MEMS Sensors: A Review of Applications, Markets and Technologies," Sensor Rev., **33/4**, pp. 300–304.

[7] Nawi, M. N. M., Manaf, A. A., Arshad, M. R., and Sidek, O., 2011, "Review of MEMS Flow Sensors Based on Artificial Hair Cell Sensor," Microsyst. Technol., **17**, pp. 1417–1426.

[8] Batra, R. C., Porfiri, M., and Spinello, D., 2006, "Electromechanical Model of Electrically Actuated Narrow Microbeams," J. Microelectromech. Syst., **15**(5), pp. 1175–1189.

[9] Caruntu, D. I., and Knecht, M. W., 2015, "Microelectromechanical Systems Cantilever Resonators Under Soft Alternating Current Voltage of Frequency Near Natural Frequency," ASME J. Dyn. Syst., Meas., Control, **137**(4), p. 041016.

[10] Zhang, W., and Meng, G., 2005, "Nonlinear Dynamical System of Micro-Cantilever Under Combined Parametric and Forcing Excitations in MEMS," Sens. Actuators A: Phys., **119**(2), pp. 291–299.

[11] Chen, X., and Wu, Z., 2017, "Review on Macromodels of MEMS Sensors and Actuators," Microsyst. Technol., **23**(10), pp. 4319–4332.

[12] Yin, T., Wang, B., Zhou, S., and Zhao, M., 2016, "A Size-Dependent Model for Beam-like MEMS Driven by Electrostatic and Piezoelectric Forces: A Variational Approach," Phys. E: Low-Dimensional Syst. Nanostruct., **84**, pp. 46–54.

[13] Nayfeh, A. H., Younis, M. I., and Abel-Rahman, E. M., 2005, "Reduced-Order Models for MEMS Applications," Nonlinear Dyn., **41**(1–3), pp. 211–236.

[14] Caruntu, D. I., Martinez, I., and Knecht, M. W., 2013, "Reduced Order Model Analysis of Frequency Response of Alternating Current Near Half Natural Frequency Electrostatically Actuated MEMS Cantilevers," ASME J. Comput. Nonlinear Dyn., **8**(3), p. 031011.

[15] Najar, F., Nayfeh, A. H., Abdel-Rahman, E. M., Choura, S., and El-Borgi, S., 2010, "Nonlinear Analysis of MEMS Electrostatic Microactuators: Primary and Secondary Resonances of the First Mode," J. Vib. Control, **16**(9), pp. 1321–1349.

[16] Abel-Rahman, E. M., and Nayfeh, A. H., 2003, "Secondary Resonances of Electrically Actuated Resonant Microsensors," J. Micromech. Microeng., **13**, pp. 491–501.

[17] Nayfeh, A. H., and Younis, M. I., 2005, "Dynamics of MEMS Resonators Under Superharmonic and Subharmonic Excitations," J. Micromech. Microeng., **15**(10), pp. 1840–1847.

[18] Al-Ghamdi, M. S., Alneamy, A. M., Park, S., Li, B., Khater, M. E., Abdel-Rahman, E. M., Heppler, G. R., and Yavuz, M., 2017, "Nonlinear Parameter Identification of a Resonant Electrostatic MEMS Actuator," Sensors, **17**(5), p. 1121.

[19] Alsaleem, F. A., Younis, M. I., and Ouakad, H. M., 2009, "On the Nonlinear Resonances and Dynamic Pull-in of Electrostatically Actuated Resonators," J. Micromech. Microeng., **19**(4), p. 045013.

[20] Dwivedy, S. K., and Kar, R. C., 1999, "Nonlinear Response of a Parametrically Excited System Using Higher-Order Method of Multiple Scales," Nonlinear Dyn., **20**(2), pp. 115–130.

[21] Nayfeh, A. H., and Mook, D. T., 1979, *Nonlinear Oscillations*, Wiley, New York.

[22] Caruntu, D. I., Martinez, I., and Taylor, K. N., 2013, "Voltage-Amplitude Response of Alternating Current Near Half Natural Frequency Electrostatically Actuated MEMS Resonators," Mech. Res. Commun., **52**, pp. 25–31.

[23] Younis, M. I., Abdel-Rahman, E. M., and Nayfeh, A., 2003, "A Reduced-Order Model for Electrically Actuated Microbeam-Based MEMS," J. Microelectromech. Syst., **12**(5), pp. 672–680.

[24] Caruntu, D. I., and Martinez, I., 2014, "Reduced Order Model of Parametric Resonance of Electrostatically Actuated MEMS Cantilever Resonators," Int. J. Non-Linear Mech., **66**, pp. 28–32.

[25] Bao, M., and Yang, H., 2007, "Squeeze Film Air Damping in MEMS," Sens. Actuators A, **136**(1), pp. 3–27.

[26] Caruntu, D. I., and Taylor, K. N., 2014, "Bifurcation Type Change of AC Electrostatically Actuated MEMS Resonators Due to DC Bias," Shock Vib., **2014**, p. 542023.

[27] Lakrad, F., and Belhaq, M., 2010, "Suppression of Pull-in Instability in MEMS Using a High-Frequency Actuation," Commun. Nonlinear Sci. Numer. Simul., **15**(11), pp. 3640–3646.

[28] Doedel, E. J., and Oldeman, B. E., 2012, *AUTO-07P: Continuation and Bifurcation Software for Ordinary Differential Equations*, Concordia University, Montreal, QC, Canada.

[29] Shampine, L. F., and Reichelt, M. W., 1997, "The MATLAB ODE Suite," SIAM: J. Sci. Comput., **18**, pp. 1–22.

[30] Shampine, L. F., Reichelt, M. W., and Kierzenka, J. A., 1999, "Solving Index-1 DAEs in MATLAB and Simulink," SIAM Rev., **41**(3), pp. 538–552.

[31] Kierzenka, J. A., and Shampine, L. F., 2001, "A BVP Solver Based on Residual Control and the MATLAB PSE," ACM Trans. Math. Software, **27**(3), pp. 299–316.

[32] Labuschagne, A., van Renburg, N. F. J., and van der Merwe, A. J., 2009, "Comparison of Linear Beam Theories," Math. Comput. Modell., **49**(1–2), pp. 20–30.

[33] Caruntu, D. I., 2007, "Classical Jacobi Polynomials, Closed-Form Solutions for Transverse Vibrations," J. Sound Vib., **306**(3–5), pp. 467–494.

[34] Caruntu, D. I., 2009, "Dynamic Modal Characteristics of Transverse Vibrations of Cantilevers of Parabolic Thickness," Mech. Res. Commun., **33**(3), pp. 391–404.

[35] Caruntu, D. I., 2013, "Factorization of Self-Adjoint Ordinary Differential Equations," Appl. Math. Comput., **219**(14), pp. 7622–7631.

[36] Nguyen, C. C., and Li, W. L., 2017, "Effect of Gas on the Quality Factors of Micro-Beam Resonators," Microsyst. Technol., **23**(8), pp. 3185–3199.

[37] Guo, X., and Alexeenko, A., 2009, "Compact Model on Rarefied Flow Simulations," J. Micromech. Microeng., **19**(4), p. 045026.

[38] Lee, J. W., Tung, R., Raman, A., Sumali, H., and Sullivan, J. P., 2009, "Squeeze-Film Damping of Flexible Microcantilevers at Low Ambient Pressures: Theory and Experiments," J. Micromech. Microeng., **19**(10), p. 105029.